AUTHOR QUERY FORM

ELSEVIER	**Book:** MACKIE-9780081004050 **Chapter:** 18	**Please e-mail your responses and any corrections to:** **E-mail: m.rajendran@elsevier.com**

Dear Author,

Any queries or remarks that have arisen during the processing of your manuscript are listed below and are highlighted by flags in the proof. (AU indicates author queries; ED indicates editor queries; and TS/TY indicates typesetter queries.) Please check your proof carefully and answer all AU queries. Mark all corrections and query answers at the appropriate place in the proof using on-screen annotation in the PDF file. For a written tutorial on how to annotate PDFs, click http://www.elsevier.com/__data/assets/pdf_file/0007/98953/Annotating-PDFs-Adobe-Reader-9-X-or-XI.pdf. A video tutorial is also available at http://www.screencast.com/t/9OIDFhihgE9a. Alternatively, you may compile them in a separate list and tick off below to indicate that you have answered the query.

Please return your input as instructed by the project manager.

Location in Chapter	Query / Remark	
AU:1, NPI	Please check the generated keywords, and correct if necessary.	☐
AU:2, page 219	Missing reference: Herman, 2010 is not listed in the 'References' section; please provide complete reference details.	☐
AU:3, page 219	Missing reference: Labow et al., 2011 is not listed in the 'References' section; please provide complete reference details.	☐
AU:4, page 228	Please replace "recent" and "recently" with specific dates.	☐
AU:5, page 228	Missing reference: Winchester, 1997 is not listed in the 'References' section; please provide complete reference details.	☐
AU:6, page 228	There were two references "Krotkov et al., 1999a" and "Krotkov et al., 1999b" found in the reference list. Hence please advise to which reference the citation "Krotkov et al., 1999" has to be linked.	☐

C H A P T E R

12

c0018

Ultraviolet Satellite Measurements of Volcanic Ash

S.A. Carn[1], N.A. Krotkov[2]

[1]Michigan Technological University, Houghton, MI, United States; [2]NASA Goddard Space Flight Center, Greenbelt, MD, United States

s0010

1. INTRODUCTION

p0010   Since the first glimpses of atmospheric aerosol from space, made in the early 1960s by Russian cosmonauts taking handheld photographs of Earth from the Vostok spacecraft (Lazarev et al., 1987; Torres and Remer, 2013), visible imagery has remained an important source of space-borne aerosol observations (eg, Kokhanovsky, 2013). More quantitative measurements from satellite-based spectrometers in the visible, infrared (IR), and ultraviolet (UV) spectral bands soon followed these early photographs, beginning a multidecadal era of passive remote sensing of aerosol from space, enabling mapping of atmospheric aerosols derived from several sources, including volcanic eruptions (eg, Seftor et al., 1997; Torres and Remer, 2013).

p0015   The earliest satellite observations of volcanic eruption clouds used single-band visible imagery from meteorological satellites such as the US National Oceanic and Atmospheric Administration (NOAA) Geostationary Operational Environmental Satellites (GOES) and Polar Operational Environmental Satellites (POES) and the Japanese Geostationary Meteorological Satellite (GMS) to track airborne ash (eg, Robock and Matson, 1983; Hanstrum and Watson, 1983; Sawada, 1987, 1989). These studies largely focused on major eruptions generating extensive ash clouds and involving stratospheric ash injection, such as the 1982 El Chichón (Mexico) and 1982 Galunggung (Indonesia) eruptions. Lacking the spectral information available from IR channels (eg, Prata, 1989), ash was identified in gray scale visible imagery based on its distinctive visible reflectance, particularly against the dark oceanic background

(eg, Robock and Matson, 1983). Analysis of cloud patterns and morphological characteristics in single-band imagery by skilled analysts remains an important method for distinguishing volcanic ash from meteorological clouds, although it can be very challenging in the tropics, where orographic cloud development can mimic the onset of an eruption. Seminal work by Sawada (1987, 1989) on eruptions in the western Pacific showed that only 31 (14%) of 227 eruptions reported within the GMS field of view over a 9-year period were subsequently identified in GMS imagery, although all clouds that exceeded 10 km altitude above sea level (asl) were detected (Oppenheimer, 1998). Many ash plumes are of limited extent (perhaps smaller than a typical kilometer-scale satellite pixel), optically thin, and/or mixed with or below meteorological clouds, requiring more advanced techniques for detection. Whilst serendipitous photographs of volcanic ash plumes from space or visible satellite imagery still provide some of the most compelling views of volcanic ash plumes (eg, Fig. 1), they are largely nonquantitative and provide minimal information for mitigation of volcanic ash hazards to aviation.

p0020   After early analyses of visible satellite imagery of volcanic ash clouds, multispectral IR techniques for ash detection and retrieval of volcanic ash mass loading were developed (eg, Prata, 1989; Wen and Rose, 1994), and subsequently became the mainstay of operational volcanic ash detection procedures used by volcanic ash advisory centers (VAACs). The potential for UV satellite observations of atmospheric aerosol, including volcanic ash, was first realized in the late 1990s, using data from the Total Ozone Mapping Spectrometer (TOMS) instrument (Hsu et al., 1996; Herman et al., 1997; Krotkov et al., 1997; Seftor et al., 1997; Torres et al., 1998). However, the obvious drawback of the UV measurements for timely volcanic ash detection and tracking is their restriction to daytime periods and coarser spatial resolution than IR data, which has limited their operational application. Nevertheless, during daytime, UV measurements offer some key advantages over IR techniques, particularly in cloudy conditions when UV-absorbing aerosol can be detected above meteorological cloud decks or mixed with clouds. In contrast, IR ash detection usually requires that the volcanic ash is the highest cloud layer in the scene (eg, Pavolonis et al., 2013). In clear-sky conditions, UV techniques can detect aerosol through the total atmospheric column, whereas IR methods are less sensitive to lower tropospheric aerosol due to thermal contrast constraints (eg, Prata and Grant, 2001). UV measurements are also less sensitive to surface reflectance than visible techniques; the latter are typically limited over land due to the highly variable surface albedo, whereas the surface albedo in the UV is relatively low and uniform (in the absence of snow or ice), and most of the UV radiance observed at satellite originates from atmospheric Rayleigh scattering. All UV satellite sensors can also provide simultaneous measurements of sulfur dioxide (SO_2) and volcanic ash, permitting distinction between magmatic eruptions, which produce SO_2 and ash emissions at high altitudes and are the major hazard to aviation (eg, Casadevall, 1994; Prata and Tupper, 2009); phreatic eruptions, which may emit ash at lower tropospheric altitudes but no SO_2 and are less hazardous; and effusive eruptions,

f0010   **FIGURE 1**   Spectacular view of the developing eruption cloud from Sarychev Peak (Kurile Islands, Russia) on June 12, 2009, at 22:16 GMT, taken by astronauts on the International Space Station (ISS) Expedition 20 from ∼400 km altitude. *Image courtesy of the Earth Science and Remote Sensing Unit, National Aeronautics and Space Administration (NASA) Johnson Space Center (available from: http://eol.jsc.nasa.gov/SearchPhotos/photo.pl? mission=ISS020&roll=E&frame=9048).*

VI. OBSERVING AIRBORNE ASH FROM SPACE

which produce copious tropospheric SO_2 emissions but minimal ash and hence also pose little threat to aircraft at cruising altitudes. Furthermore, the relative simplicity of the UV Aerosol Index (UVAI) algorithm described below permits its application to a large family of UV sensors (Table 1), including TOMS (1978–2005), the Global Ozone Monitoring Experiment (GOME, GOME-2; 1995–present), the Scanning Imaging Absorption Spectrometer for Atmospheric Chartography (SCIAMACHY; 2002–12), the Ozone Monitoring Instrument (OMI; 2004–present), the Ozone Mapping and Profiler Suite (OMPS; 2012–present), the recently launched Earth Polychromatic Imaging Camera (EPIC) aboard the Deep Space Climate Observatory (DSCOVR; 2015–) and the future Tropospheric Monitoring Instrument (TROPOMI; scheduled for launch in 2016 on the Sentinel-5 Precursor satellite). This allows the generation of long-term, consistent UV aerosol records and climatologies.

p0025   In addition to the mitigation of volcanic ash hazards to aviation, the mapping and quantification of UV-absorbing aerosols such as volcanic ash is of wider importance for several reasons. Earth's radiation balance (ie, climate), heterogeneous atmospheric chemical reactions (eg, ozone destruction), the surface UV flux (which impacts human health via erythemal daily surface UV doses and drives some of the photochemical reactions that produce air pollution), and marine biogeochemistry (ie, the global carbon cycle) are all impacted by the presence of UV-absorbing aerosols in the atmosphere. Except for a few hours or days after a major explosive eruption, volcanic ash emitted by sporadic smaller eruptions is a relatively minor constituent of the total atmospheric loading of UV-absorbing aerosol at any given time. UV-absorbing aerosol abundance in the atmosphere is dominantly controlled by several large, seasonally variable sources of aerosols distributed over large areas by tropospheric winds, including biomass burning smoke plumes (sourced from mid-to high-latitude forests in Siberia, North America, and Australia in summer and from equatorial regions in the dry season) and desert mineral dust. Simultaneous UV measurements of SO_2 and aerosol provide a means to distinguish volcanic ash from these other aerosol types, provided that the volcanic SO_2 and ash remain approximately collocated. In this review, we focus on UV measurements of volcanic ash; descriptions of aerosol measurement techniques using satellite observations at visible wavelengths are provided by Kahn et al. (2007), Kahn and Limbacher (2012), Winker et al. (2012), Kokhanovsky (2013), and Torres and Remer (2013).

s0015   ## 2. ULTRAVIOLET ASH DETECTION AND RETRIEVAL ALGORITHMS

s0020 ### 2.1 The Ultraviolet Aerosol Index

p0030   The UV Aerosol Index (UVAI or AI) is the most common quantity used to track volcanic ash clouds using UV satellite measurements (eg, Fig. 2). Satellite measurements of UV radiation backscattered from the Earth's atmosphere and surface are primarily used to retrieve atmospheric column amounts of ozone. However, during the TOMS missions, it was discovered that the presence of other interfering species that also absorb UV radiation, notably volcanic SO_2 and absorbing aerosols, impacted the ozone measurements, and hence, corrections were needed to achieve the stringent requirements for ozone retrieval precision. Thus, in a similar origin to UV satellite measurements of SO_2, development of the UVAI arose from the need to correct UV TOMS ozone retrievals for the effects of aerosol absorption, and was first proposed in the late 1990s (Hsu et al., 1996; Herman et al., 1997; Seftor et al., 1997; Torres et al., 1998). Hsu et al. (1996) reported the first detection of smoke from biomass burning in UV TOMS measurements based on reflectivity differences between TOMS channels at 340 and 380 nm, which they termed a "smoke index," although they did not discuss applications to volcanic ash detection.

p0035   The first step in most UV retrieval algorithms (ozone, SO_2, trace gases, or aerosols) is calculation of the effective UV reflectivity for each scene at a nonabsorbed (ie, >340 nm) wavelength. Several reflectivity models representing the geophysical conditions of a UV satellite observation of the Earth–atmosphere system exist, generally referred to as Lambertian equivalent reflectivity (LER) models. The simplified LER (SLER) model (Chandrasekhar, 1960; Dave, 1964; Krotkov et al., 2001; Herman, 2010; Labow et al., 2011) involves fitting the at-satellite measured radiance at a [**AU2**][**AU3** nonabsorbed wavelength (I_{meas}) with the calculated radiance, assuming a pure Rayleigh atmosphere bounded by a Lambertian surface at a surface pressure of $P_{surf} = 1$ atm:

$$I_{meas} = I_0 + \frac{R \cdot T}{[1 - R \cdot S_b]}$$ [1]

where R (SLER) is the effective albedo of an ideal Lambertian reflecting surface, representing a mixed surface/cloud scene at a specific satellite viewing geometry; I_0 is the theoretical pure Rayleigh atmospheric radiance without any

t0010 **TABLE 1**   Current (June 2015) and Near-Future Satellite Missions With UV/Visible Volcanic Ash Imaging or Monitoring Capabilities

Satellite[a]	Sensor(s)[b]	Launch date	Monitoring capability	Overpass time (local)[b]	Resolution Spatial (nadir)[c]	Resolution Temporal[d]	Websites[e]
POLAR-ORBITING (LEO) − VISIBLE							
NOAA-15	AVHRR/3	May 13, 1998	Ash, aerosols	7:30 am	1 km	Daily	USGS: http://volcview.wr.usgs.gov/
Landsat 7	ETM+	Apr. 15, 1999	Ash, aerosols	9:45 am	15−60 m	16 days	Landsat Science: http://landsat.gsfc.nasa.gov/
NASA Terra	MODIS ASTER MISR	Dec. 18, 1999	Ash, aerosols Ash, aerosols Ash plumes (altitude)	10:30 am	250 m 15 250−275 m	2 × daily 16 days 9 days	https://worldview.earthdata.nasa.gov/ AVA: http://ava.jpl.nasa.gov/ MISR at JPL: http://www-misr.jpl.nasa.gov/
NASA EO-1	ALI Hyperion	Nov. 21, 2000	Ash, aerosols Ash, aerosols	10:00 am	10−30 m 30 m	16 days 16 days	USGS: http://eo1.usgs.gov/
NASA Aqua	MODIS	May 4, 2002	Ash, aerosols	1:30 pm	250 m	2 × daily	https://worldview.earthdata.nasa.gov/
NOAA-18	AVHRR/3	May 20, 2005	Ash, aerosols	1:30−2:30 pm	1 km	Daily	USGS: http://volcview.wr.usgs.gov/
CALIPSO	CALIOP	Apr. 28, 2006	Ash/aerosol cloud altitude	1:31 pm	333 m (horiz.)	16 days	http://www-calipso.larc.nasa.gov/
EUMETSAT MetOp-A	AVHRR/3	Oct. 29, 2006	Ash, aerosols	9:30 am	1 km	Daily	http://www.nsof.class.noaa.gov/
NOAA-19	AVHRR/3	Feb. 6, 2009	Ash, aerosols	1:30−2:30 pm	1 km	Daily	USGS: http://volcview.wr.usgs.gov/
NASA/NOAA Suomi NPP	VIIRS	Oct. 29, 2011	Ash, aerosols	1:30 pm	375−750 m	2 × daily	http://viirsland.gsfc.nasa.gov/index.html
EUMETSAT MetOp-B	AVHRR/3	Sep. 17, 2012	Ash, aerosols	9:30 am	1 km	Daily	http://www.nsof.class.noaa.gov/
Landsat 8	OLI	Feb. 11, 2013	Ash, aerosols	10:00 am	15−100 m	16 days	USGS: http://landsat.usgs.gov/landsat8.php
ESA Sentinel-2A	MSI	Jun. 23, 2015	Ash, aerosols	10:30 am	10−60 m	5 days	https://earth.esa.int/web/sentinel/missions/sentinel-2
POLAR-ORBITING (LEO) − ULTRAVIOLET							
NASA Aura	OMI	Jul. 15, 2004	SO_2, ash, aerosols	1:45 pm	13 × 24 km	∼Daily	NASA: http://so2.gsfc.nasa.gov/
EUMETSAT MetOp-A	GOME-2A	Oct. 19, 2006	SO_2, ash, aerosols	9:30 am	80 × 40 km	∼Daily	SACS: http://sacs.aeronomie.be/nrt/
NASA/NOAA Suomi NPP	OMPS	Oct. 29, 2011	SO_2, ash, aerosols	1:30 pm	10−50 km	Daily	NASA: http://so2.gsfc.nasa.gov/

EUMETSAT MetOp-B	GOME-2B	Sep. 17, 2012	SO_2, ash, aerosols	9:30 am	80×40 km	~ Daily	SACS: http://sacs.aeronomie.be/nrt/
ESA Sentinel-5 Precursor	TROPOMI	*2016*	SO_2, ash, aerosols	1:35 pm	7×7 km	Daily	http://www.tropomi.eu/
GEOSTATIONARY (GEO) − VISIBLE							
EUMETSAT Meteosat-7	MVIRI	Feb. 9, 1997	Ash, aerosols	n/a	2.5−5 km; 57°E	30 min	
CMA FY-2E	S-VISSR	Oct. 19, 2004	Ash, aerosols	n/a	1.25−5 km; 105°E	30 min	http://www.ssec.wisc.edu/data/geo/
EUMETSAT Meteosat-9	SEVIRI	Dec. 22, 2005	Ash, aerosols	n/a	1−3 km; 9.5°E	5 min	http://volcano.ssec.wisc.edu/ http://fred.nilu.no/sat/
JMA MTSAT-2	Himawari-7	Feb. 18, 2006	Ash, aerosols	n/a	1.25−5 km; 145°E	30 min	http://volcano.ssec.wisc.edu/
CMA FY-2D	S-VISSR	Nov. 15, 2006	Ash, aerosols	n/a	1.25−5 km; 87°E	30 min	http://www.ssec.wisc.edu/data/geo/
GOES-14 (E)	Imager	Jun. 27, 2009	Ash, aerosols	n/a	1−4 km; 75°W	1 min	http://volcano.ssec.wisc.edu/
GOES-15 (W)	Imager	Mar. 4, 2010	Ash, aerosols	n/a	1−4 km; 135°W	1 min	http://volcano.ssec.wisc.edu/
KMA COMS-1	MI	Jun. 26, 2010	Ash, aerosols	n/a	1−4 km; 128°E	10 min	http://www.ssec.wisc.edu/data/geo/
CMA FY-2F	S-VISSR	Jan. 13, 2012	Ash, aerosols	n/a	1.25−5 km; 113°E	30 min	
EUMETSAT Meteosat-10	SEVIRI	Jul. 5, 2012	Ash, aerosols	n/a	1−3 km; 0°	15 min	http://volcano.ssec.wisc.edu/ http://fred.nilu.no/sat/
JMA MTSAT	Himawari-8	Oct. 7, 2014	Ash, aerosols	n/a	0.5−2 km; 145°E	2.5 min	http://mscweb.kishou.go.jp/ himawari89/
GOES-R	ABI	*Early 2016*	Ash, aerosols	n/a	0.5−2 km; 75°/137°W	30 s	http://www.goes-r.gov/
L1 LAGRANGE LIBRATION POINT − UV/VISIBLE							
NOAA DSCOVR	EPIC	Feb. 11, 2015	SO_2, ash, aerosols	n/a	8 km; sunlit Earth disk	90 min	http://www.nesdis.noaa.gov/DSCOVR/

[a]Satellite and sensor acronyms: NOAA, *National Oceanic and Atmospheric Administration*; NASA, *National Aeronautics and Space Administration*; EO, *Earth Observing*; CALIPSO, *Cloud-Aerosol Lidar and Infrared Pathfinder Satellite Observations*; EUMETSAT, *European Organization for the Exploitation of Meteorological Satellites*; NPP, *National Polar-orbiting Partnership*; ESA, *European Space Agency*; CMA, *China Meteorological Administration*; FY, *Feng-Yun*; JMA, *Japan Meteorological Agency*; MTSAT, *Multifunctional Transport SATellite*; GOES, *Geostationary Operational Environmental Satellite*; KMA, *Korean Meteorological Administration*; COMS, *Communication, Ocean and Meteorological Satellite*; DSCOVR, *Deep Space Climate ObserVatoRy*; AVHRR, *Advanced Very High Resolution Radiometer*; ETM, *Enhanced Thematic Mapper*; MODIS, *MODerate resolution Imaging Spectroradiometer*; ASTER, *Advanced Spaceborne Thermal Emission and Reflection radiometer*; MISR, *Multiangle Imaging SpectroRadiometer*; ALI, *Advanced Land Imager*; OMI, *Ozone Monitoring Instrument*; CALIOP, *Cloud-Aerosol Lidar with Orthogonal Polarization*; GOME, *Global Ozone Monitoring Experiment*; OMPS, *Ozone Mapping and Profiler Suite*; VIIRS, *Visible Infrared Imaging Radiometer Suite*; OLI, *Operational Land Imager*; MSI, *MultiSpectral Imager*; TROPOMI, *TROPOspheric Monitoring Instrument*; MVIRI, *Meteosat Visible and Infrared Imager*; S-VISSR, *Stretched Visible and Infrared Spin Scan Radiometer*; SEVIRI, *Spinning Enhanced Visible and InfraRed Imager*; MI, *Meteorological Imager*; ABI, *Advanced Baseline Imager*; EPIC, *Earth Polychromatic Imaging Camera*.
[b]Only the daytime overpass of each satellite is given.
[c]Spatial resolution typically varies between spectral bands.
[d]The maximum temporal resolution is listed. Some LEO spacecraft/sensors are pointable (eg, NASA's EO-1, Terra/ASTER), which can increase temporal resolution. Note that geostationary imagers typically have a nominal temporal resolution of 15−30 min, but higher resolution is possible in special observation modes (eg, GOES Super Rapid Scan).
[e]URLs provided are examples of sites where instrumental datasets (if available) can be viewed or accessed (URLs were active at the time of writing).

f0015 **FIGURE 2** Hemispheric transport of volcanic ash from the June 2011 eruption of Cordón Caulle (Chile) observed by OMI. Ash transport was tracked using the OMI UV Aerosol Index (UVAI). The sequence of images shows daily OMI UVAI maps from June 5–13, 2011, as the Cordón Caulle volcanic ash cloud drifted eastwards around the globe from Chile. Darker tones represent higher values of UVAI. *Image created by Colin Seftor (http://acdb-ext.gsfc.nasa.gov/People/Seftor/puyehue.html).*

surface contribution (ie, path radiance); S_b is the albedo of the Rayleigh atmosphere illuminated isotropically from below; and $T = F_d f$, where F_d is the total downwelling surface irradiance (direct plus diffuse), and f is the fraction of the upwelling radiance reaching the satellite (ie, the directional atmospheric transmittance for isotropic illumination from below: $f = I_{TOA}/I_{surf}$; where TOA = top of the atmosphere). The quantities I_0, S_b, F_d, and f are precalculated using radiative transfer models of Rayleigh scattering. Results from TOMS and OMI show that the reflectivity R has little spectral (wavelength) dependence, except in the presence of UV-absorbing aerosols. Observed reflectivity differences between different UV wavelengths ($\Delta R = R_{\lambda 0} - R_\lambda$), essentially indicating that the SLER approximation (or the equivalent model in use at the time) is not adequately representing all the radiative transfer effects, revealed the first evidence for the effects of absorbing aerosols on TOMS measurements (Hsu et al., 1996).

p0040   To eliminate the large angular dependencies (ie, with satellite viewing angle) of reflectivity measurements, Herman et al. (1997) subsequently defined the AI in terms of UV radiances as the difference between the measured and calculated spectral contrast:

$$\text{AI} = -100 \log \left[\left(\frac{I_\lambda}{I_{\lambda_0}} \right)_{\text{obs}} - \left(\frac{I_\lambda}{I_{\lambda_0}} \right)_{\text{calc}} \right] \qquad [2]$$

where I_{obs} and I_{calc} represent observed and calculated backscattered radiances at two UV wavelengths, λ and λ_0, in the 330–380 nm range (where ozone absorption is negligible; initially 340 and 380 nm were used), respectively. However, since the calculation of UV effective reflectivity (1) requires that $(I_{\lambda 0})_{\text{obs}} = (I_{\lambda 0})_{\text{calc}}$, the UVAI reduces to:

$$\text{AI} = -100 \log \left[\frac{(I_\lambda)_{\text{obs}}}{(I_\lambda)_{\text{calc}}} \right] \qquad [3]$$

VI. OBSERVING AIRBORNE ASH FROM SPACE

where $\lambda = 340$ nm for the first Nimbus-7 TOMS UVAI measurements. In the presence of UV-absorbing aerosols such as volcanic ash (or smoke, desert dust), I_{obs} is reduced relative to I_{calc}, and a positive residue (or AI) results, indicating reduced backscatter relative to a molecular (Rayleigh scattering) atmosphere. Conversely, if nonabsorbing (scattering) aerosols dominate (eg, sulfate aerosol), enhancing atmospheric backscatter, then the radiance residual (AI) is negative. However, the dynamic range of negative UVAI values is much lower than for positive values and depends on aerosol optical depth and particle size (Torres et al., 1998). A unit AI value represents a 2.3% radiance change (ie, a reduction in the case of absorbing aerosol, such as volcanic ash).

p0045   Following discovery of the UVAI technique, Seftor et al. (1997) reported the first application of the technique to volcanic ash, using UVAI measurements to track ash emitted by the April 4, 1982, eruption of El Chichón (Mexico) for ~4 days. They found good agreement between UVAI ash maps and observations from visible and IR satellite sensors, and also noted significant geographical separation of the ash and SO_2 clouds generated by the eruption, which they attributed to vertical wind shear acting on ash and SO_2 clouds residing at different altitudes (Seftor et al., 1997), later proposed to be the result of gravitational separation of ash and SO_2 (Schneider et al., 1999). Although first proposed using TOMS measurements, the UVAI concept for aerosol detection has subsequently been applied to other near-UV satellite instruments including GOME (Gleason et al., 1998; de Graaf et al., 2005), SCIAMACHY (Penning de Vries et al., 2009; de Graaf et al., 2007), OMI (Torres et al., 2007; Ahn et al., 2008; Dirksen et al., 2009, Fig. 2), and GOME-2. The OMI UVAI is calculated using $\lambda = 331$ nm or 354 nm in Eq. 2 (Torres et al., 2007), and it is important to note that the exact value of the UVAI depends on the wavelength used, in addition to other factors such as the spatial resolution of the sensor (since UVAI is averaged over the instrument field of view).

p0050   There are many advantages of the UVAI technique for detecting and tracking volcanic ash clouds (eg, compared to visible or IR techniques). Meteorological clouds (comprised of large, nonabsorbing particles with near-zero Angstrom coefficients) produce near-zero UVAI values; thus, ash detection is not impacted by underlying clouds, and ash can be detected above cloud decks or intermingled with clouds. In contrast, IR-based techniques generally require that the ash cloud is the highest cloud layer in a scene (eg, Pavolonis et al., 2013). Since the UV reflectance of all terrestrial surfaces (in the absence of snow or ice) is small and relatively invariant, the detection of ash and potential retrieval of ash properties is possible over a larger range of land surfaces than in the visible, including arid and semiarid regions that appear very bright in the visible and near-IR. The UVAI can be derived over land or water (unlike some visible reflectance-based methods), including bright terrestrial surfaces such as ice/snow (IR techniques tend to be restricted in such conditions). The UVAI can also detect volcanic ash at any altitude in clear-sky conditions, whereas ash detection using the IR split-window technique requires thermal contrast between the ash layer and the underlying surface (eg, Prata and Grant, 2001), and can distinguish between absorbing aerosol (ie, ash) and nonabsorbing particles (eg, sulfate aerosol) through the sign of the UVAI. The magnitude of the UVAI for volcanic ash is dependent on ash layer altitude, optical depth, particle size distribution, and single scattering albedo. All else being equal, ash at higher altitude produces a higher UVAI; ash (or other absorbing aerosols such as smoke) at altitudes of 10 km asl or above yield particularly high UVAI values (up to 30 or more) that are diagnostic of upper tropospheric or stratospheric aerosols (eg, Torres et al., 2007). The relative simplicity and flexibility of the UVAI algorithm permits its application to a large family of past, present, and future UV satellite sensors (eg, TOMS, GOME, SCIAMACHY, OMI, OMPS, GOME-2, EPIC, TROPOMI) and the generation of long-term consistent aerosol climatologies. Furthermore, all UV satellite instruments can also provide simultaneous measurements of SO_2 and UVAI, permitting tracking of the two most important constituents of volcanic clouds and assessment of their spatial relationships.

p0055   Disadvantages of the UVAI for volcanic ash detection include nonspecificity to volcanic ash, since the technique is sensitive to any UV-absorbing aerosols including smoke (carbonaceous aerosol), desert mineral dust, or anthropogenic pollution. This contrasts with the IR split-window ash detection technique, which exploits silicate absorption features at wavelengths of 10−12 μm and is hence specifically tuned to silicate aerosols such as volcanic ash (Prata, 1989). Hence, where multiple sources of absorbing aerosols are present, it may be difficult to distinguish volcanic ash from smoke or dust, although coincident SO_2 data can provide definitive identification and location of volcanic clouds if the SO_2 and ash have not separated in the horizontal. The UVAI is also a daytime-only measurement and only provides semiquantitative information on volcanic ash (increasing UVAI can indicate increasing ash concentrations, ash altitude, or both), although more quantitative retrievals of ash properties are possible (Section 2.2). Uncorrected spectral variations in surface reflectance, particularly sunglint over the oceans, can result in UVAI artifacts, but these are usually screened from UVAI datasets or occur in predictable locations. Sunglint is more problematic (causing more UVAI data loss over oceans) for early afternoon satellite overpasses (lower solar zenith angle; eg, OMI) than for morning overpasses (eg, GOME-2). Ocean color effects can also produce both positive and

negative residues of magnitude less than one UVAI unit; eg, pure water absorption and colored dissolved organic matter in the remote oceans may yield UVAI values as high as 0.7, whereas chlorophyll absorption in coastal waters produces negative residues of about the same magnitude (Torres and Remer, 2013). However, such noise in UVAI data over oceans does not seriously impact the detection of volcanic ash since the magnitude of the UVAI in upper tropospheric or lower stratospheric (UTLS) volcanic ash plumes is typically several times larger than the background ocean signal. UVAI measurements are also sensitive to the absolute calibration of UV satellite instruments.

p0060   Near real-time (NRT) UVAI observations of volcanic ash (and SO$_2$) from currently operational satellite instruments (OMI, GOME-2, OMPS; Table 1) can be accessed on several websites including the Satellite Measurements from Polar Orbit (SAMPO) system developed by the Finnish Meteorological Institute (FMI), which exploits direct broadcast data from the Aura satellite to reduce data latency (FMI, 2014), the NOAA NRT OMI website (NOAA, 2015), the Support to Aviation Control Service (SACS; BIRA, 2015), and the Tropospheric Emission Monitoring Internet Service (TEMIS; ESA, 2015).

s0025 2.2 Ultraviolet Ash Optical Depth and Mass Retrievals

p0065   Although the UVAI is a very effective technique for detecting and tracking volcanic ash clouds (eg, Fig. 2), it is only semiquantitative and is dependent on aerosol abundance and altitude. Quantitative estimates of aerosol extinction optical depth (τ) and single-scattering albedo (ω) at UV wavelengths require application of an inversion algorithm to near-UV satellite observations (eg, Krotkov et al., 1997; Torres et al., 1998). The microphysical properties of atmospheric aerosol are highly variable, and hence the general inversion algorithm approach is to use precomputed UV reflectances for a set of assumed microphysical aerosol models. Since volcanic ash is only a transient aerosol species in the atmosphere, the three major aerosol types considered in operational algorithms are desert dust, carbonaceous aerosols associated with biomass burning, and weakly absorbing sulfate aerosols, which have distinct absorption and scattering properties. The aerosol extinction optical depth and single scattering albedo can be retrieved based on the variability of the relationship between the 340–380 nm spectral contrast and the 380 nm reflectance. Since the retrieval procedure is sensitive to the aerosol vertical distribution, the aerosol layer height must be assumed, and the choice of vertical distribution also varies with aerosol type and location (Torres et al., 2002). Since 2006, improved constraints on aerosol altitude and type from NASA's afternoon satellite constellation (A-Train) observations (eg, from the Cloud-Aerosol Lidar with Orthogonal Polarization (CALIOP) and Atmospheric Infrared Sounder (AIRS)) have resulted in more accurate aerosol retrievals by the operational OMI aerosol algorithm (OMAERUV; eg, Torres et al., 2013). Direct measurements of aerosol layer altitude from the CALIOP lidar have been particularly valuable, though aerosol altitude information can also be derived using the absorption of the O$_2$–O$_2$ dimer collision complex at 477 nm in the visible band.

s0030 2.2.1 Multispectral Ultraviolet Volcanic Ash Retrievals

p0070   In some cases, the UVAI alone may be sufficient to assess the aviation hazard posed by a volcanic ash cloud if the aim is to avoid any significant airborne volcanic ash. However, more accurate delineation of volcanic ash hazard zones, and estimation of the erupted ash mass, requires quantitative retrievals of ash mass loading. Retrieval of volcanic ash optical depth and mass loading is a particularly complex, underdetermined problem due to the highly variable optical properties of ash particles (ie, the spectral refractive index, $m(\lambda)$), which depend on ash composition (eg, Fig. 4), particle size distribution, and ash particle shape, in addition to the dependence on ash layer altitude. A further source of uncertainty is the heterogeneous nature of "volcanic ash" itself, which may comprise some or all of shards of volcanic glass, fragmented bubble walls, crystal fragments, and lithic clasts, some or all of which may be coated by and/or mixed with condensed water, ice, or acid droplets (eg, Farlow et al., 1981; Rose et al., 2000; Guo et al., 2004). Thus, several assumptions are required in the retrieval algorithm and a limited number of parameters can be retrieved, precluding NRT volcanic ash retrievals. Currently, a major impediment to wider application of UV ash retrievals is the paucity of ash refractive index data in the UV–visible wavelength range for a range of volcanic ash compositions.

p0075   As described above (Section 2.1), volcanic ash clouds can be accurately located in UV satellite data by discrimination from the Rayleigh scattering atmosphere using the UVAI. Quantitative retrieval of ash optical depth, effective particle size, and mass loading can then be achieved by fitting measured and simulated UVAI values in these pixels (eg, Krotkov et al., 1999a, Fig. 3). The general approach for multispectral UV measurements (eg, TOMS) is as follows. Firstly, the scattering properties of the ash particles must be calculated at the two wavelengths used to calculate the UVAI (eg, 340 and 380 nm for TOMS) using Mie theory. The key (and unrealistic) assumption involved here is that
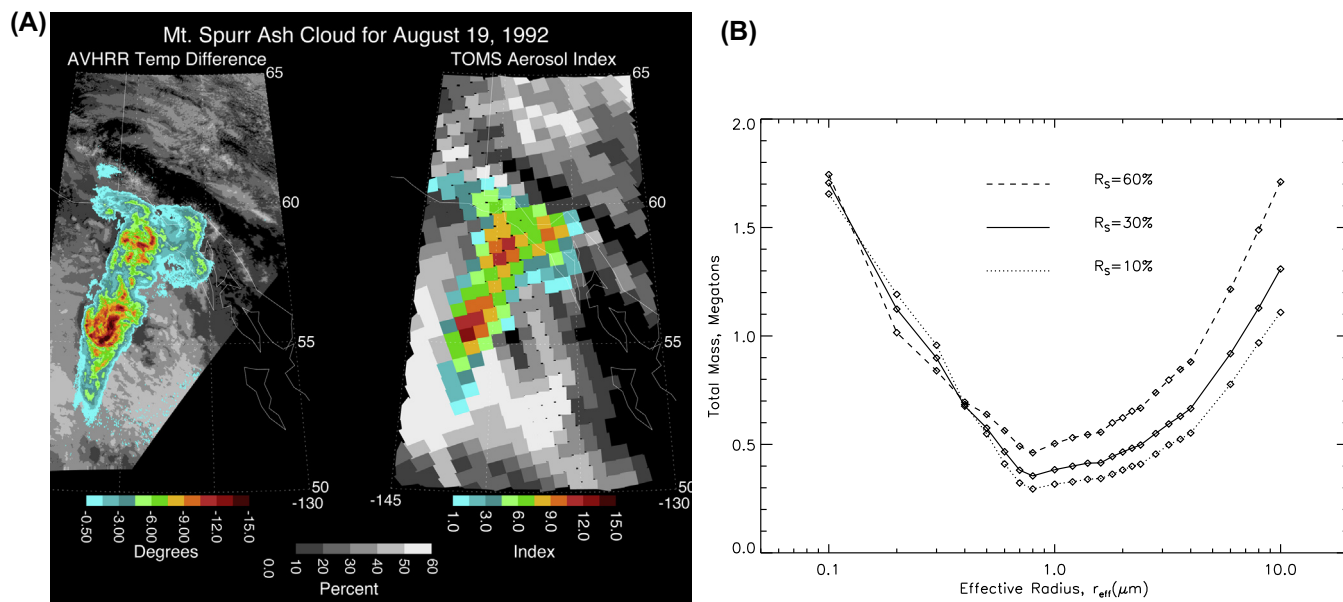
f0020 **FIGURE 3** (A) Comparison of IR brightness temperature difference (AVHRR) and UVAI (Nimbus-7 TOMS) data from the August 18, 1992, eruption of Mt. Spurr (Alaska) observed on August 19, 1992, at 18:57 UTC. The AVHRR 10.8 and 12 μm brightness temperature data are measured with 1 km spatial resolution. Underlying water clouds are shown in gray scale beneath the ash cloud. The TOMS 0.38 μm (reflectivity) band is used to measure the UV reflectivity of water clouds and Earth's surface; (B) Derived TOMS total ash cloud mass as a function of assumed ash particle effective radius (r_{eff}) and reflectivity of underlying clouds (R_s). *Reproduced from Krotkov, N.A., Torres, O., Seftor, C., Krueger, A. J., Kostinski, A., Rose, W.I., Bluth, G.J.S., Schneider, D., Schaefer, S.J., 1999a. Comparison of TOMS and AVHRR volcanic ash retrievals from the August 1992 eruption of Mt. Spurr, Geophys. Res. Lett. 26(4), 455–458.*

the ash particles are homogeneous, isotropic spheres. The ash particle size distribution (which determines the particle effective radius, r_{eff}) and the complex refractive index of the ash particles at the two wavelengths must also be assumed; in the case of the August 1992 Mt. Spurr (Alaska) volcanic ash retrievals described by Krotkov et al. (1999a), actual erupted ash samples were used to determine $m(\lambda)$, but more typically, it must be assumed based on the predicted or known ash composition and a limited database of $m(\lambda)$ measurements for volcanic ash in the UV (eg, Patterson, 1981; Patterson et al., 1983). The ash particle size distribution is commonly assumed to be lognormal, though it is possible that this could change as a volcanic cloud evolves during atmospheric transport. Once the ash scattering properties have been computed, a radiative transfer model is employed to simulate the back-scattered top-of-the-atmosphere radiances at the UV wavelengths by embedding the volcanic ash layer at an assumed altitude in a molecular atmosphere above an underlying surface with assumed reflectivity (R_s), and to derive the simulated UVAI. Krotkov et al. (1999a) found that the simulated UVAI increased with both ash optical depth and ash particle effective radius (in the 0.1–10 μm range). Ash optical depths can be retrieved by finding the best fit between measured and simulated UVAI for each assumed value of R_s and r_{eff}, with the ash mass (M) in each pixel calculated thus:

$$M = \sum \frac{4}{3} \rho A r_{eff} \tau f(r_{eff}) \qquad [4]$$

where ρ is the assumed ash particle density (also dependent on composition), A is the pixel area, and f is a dimensionless mass conversion factor (averaging over the particle size distribution). Although the range of retrieved ash mass was fairly large when accounting for the entire R_s and r_{eff} parameter space, Krotkov et al. (1999a) found good agreement between UV TOMS and IR advanced very high resolution radiometer (AVHRR) ash retrievals for the 1992 Mt. Spurr volcanic eruption cloud (Fig. 3). Few other detailed comparisons between UV and IR ash retrievals have been conducted to date.

p0080   Krotkov et al. (1999b) evaluated the effects of ash particle nonsphericity on ash retrievals, and concluded that the errors associated with the use of Mie theory (ie, spherical particles) are relatively small compared to other sources of uncertainty (eg, refractive index, ash cloud altitude, ash mixtures with water, sulfate aerosol droplets, and ice). The complex refractive index alone can vary by at least two orders of magnitude between ash samples (Fig. 4; eg, Pollack et al., 1973; Patterson, 1981; Patterson et al., 1983), although such measurements remain limited in the UV–visible

VI. OBSERVING AIRBORNE ASH FROM SPACE
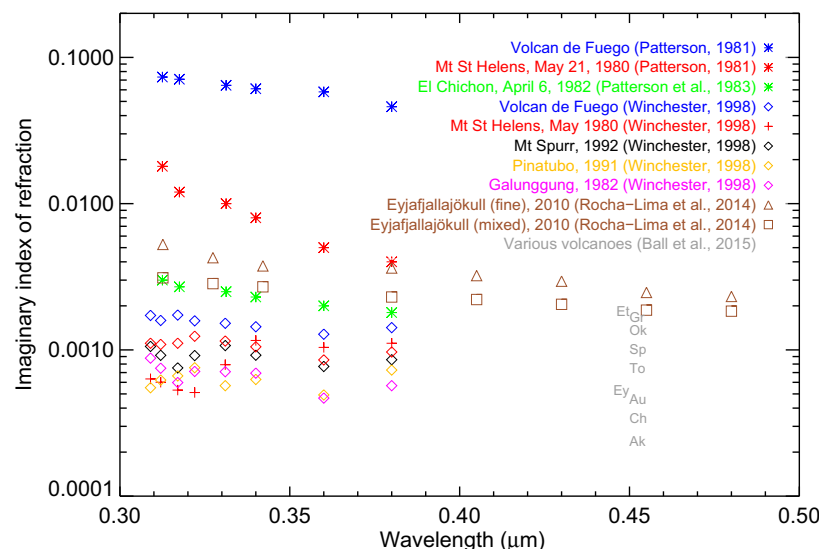
f0025 **FIGURE 4** The imaginary refractive index (*k*) of volcanic ash samples of varying composition (basalt to rhyolite) at UV and visible (blue) wavelengths, measured using different techniques. *(Data for Eyjafjallajökull ash from Rocha-Lima, A., Martins, J.V., Remer, L.A., Krotkov, N.A., Tabacniks, M.H., Ben-Ami, Y., Artaxo, P., 2014. Optical, microphysical and compositional properties of the Eyjafjallajökull volcanic ash, Atmos. Chem. Phys. 14, 10649–10661,* http://dx.doi.org/10.5194/acp-14-10649-2014.*)* are provided for fine (<2 μm diameter) and mixed (coarse + fine; <11 μm diameter) particles; uncertainties on *k* are typically ∼10–20%. Values of *k* at 0.45 μm measured by Ball et al. (2015) are shown for volcanic ash samples from: Grimsvötn 2011 (Gr), Okmok 2008 (Ok), Mt. Spurr 1992 (Sp), Tongariro 2012 (To), Eyjafjallajökull 2010 (Ey), Augustine 2006 (Au), Chaitén 2008 (Ch), Askja 1875 (Ak), and Etna 2002 (Et); all values were measured at 0.45 μm, though some symbols are offset for clarity.

wavelength range (see Section 2.2.2). Scattering matrices of some volcanic ash samples have also been measured in the lab (Munoz et al., 2004). A scattering matrix is used to track changes in polarization of radiation during scattering processes and is required for more accurate, fully polarized treatments of radiative transfer in certain spectral bands, including the UV. The key result of Munoz et al. (2004) was that all measured scattering matrix elements were confined to rather limited domains as functions of scattering angle, permitting construction of an average scattering matrix for volcanic ash as a function of the scattering angle. Such an average scattering matrix could be used for ash retrievals when the actual properties of volcanic ash (particle size and shape distributions) are not known, as is commonly the case soon after eruptions, and should improve retrievals relative to the spherical particle assumption. A further development since the work of Krotkov et al. (1999a,b) has been the availability of accurate ash layer altitude measurements from the CALIOP lidar in the A-Train (eg, Fig. 5; Winker et al., 2012), which should further reduce the uncertainty on UV ash retrievals. Fig. 5 shows vertically resolved A-Train measurements of aerosols, clouds, and trace gases (SO_2 and hydrogen chloride (HCl)) in the volcanic cloud generated by the August 2008 eruption of Kasatochi volcano (Alaska). Here, the nadir OMI measurements of positive UVAI are spatially collocated with the aerosol layers detected by CALIOP (indicating that the layers likely contain volcanic ash), but the active lidar observations reveal a multilayered structure in the volcanic cloud that is not detectable in the passive OMI measurements.

s0035 2.2.2 *Ash Optical Properties in the Ultraviolet*

p0085   There have been several recent efforts to determine the UV (and visible) optical properties of a larger number of volcanic ash samples from a range of eruptions (eg, Rocha-Lima et al., 2014; Ball et al., 2015). Laboratory measurements are conducted on ash fallout samples, usually compressed in pellets, resuspended on filters, or immersed into liquids with known refractive index. As noted above, the most important optical characteristic related to ash composition is the refractive index, $m(\lambda)$, which is specified as a complex number ($m = n - ik$) expressing refraction (scattering) as a real component, n, and absorption by an imaginary component, k. The refractive index is determined by ash composition and is wavelength dependent. It can be specified for individual particles, but in remote sensing, a single value is assumed for the entire volcanic ash column (Krotkov et al., 1999a,b). Laboratory measurement techniques for $m(\lambda)$ determination can be broadly classified into reflectance (Egan and Becker, 1969; Winchester, 1998; Rocha-Lima et al., 2014) and transmittance techniques, including single particle analysis using liquid immersion (Wahlstrom, 1974) or a combination of both (Pollack et al., 1973; Patterson, 1981; Patterson et al., 1983).
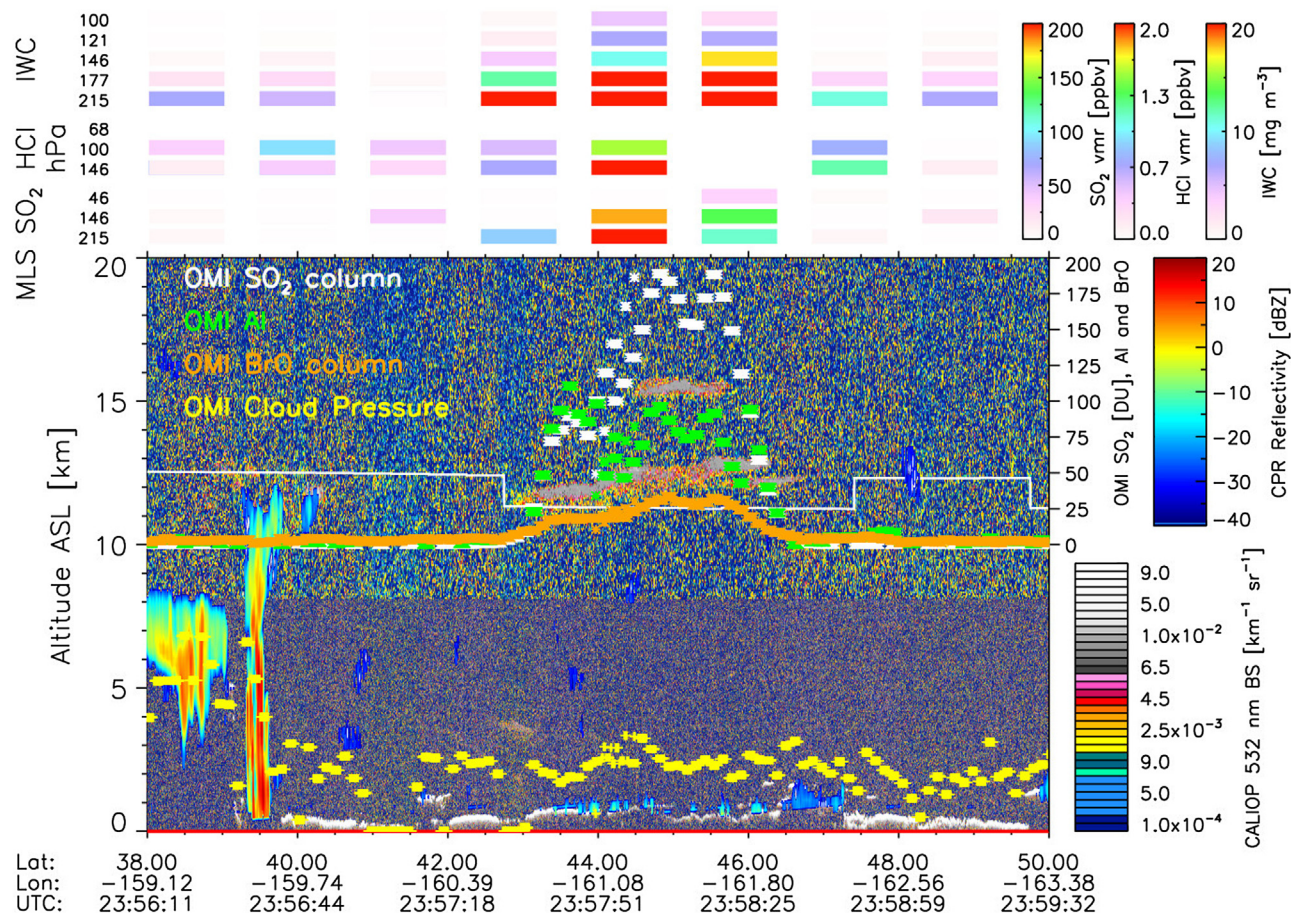
f0030 **FIGURE 5**   Example of NASA A-Train satellite sensor synergy for characterizing volcanic cloud altitude and SO$_2$ and ash abundance. Composite of daytime A-Train measurements of the Kasatochi volcanic plume on August 9, 2008, at ~23:25 UTC. Main panel shows 532 nm total attenuated backscatter (km/sr) from CALIOP, clearly showing two prominent layers of aerosol in the volcanic cloud, overlain with reflectivity from the CloudSat Cloud Profiling Radar (CPR), which, in this case, only detects hydrometeors in the tropospheric meteorological clouds (indicating that the volcanic aerosol particle size is below the radar detection limit, ie, sub-mm). *White*, *green*, *orange*, and *yellow stars* show OMI SO$_2$, UVAI, BrO, and cloud pressure measurements along the A-Train orbit track. OMI UVAI values have been multiplied by five for display (ie, the maximum UVAI = ~20). Note the correlation between SO$_2$ and UVAI data and between the UVAI and the aerosol layers detected by CALIOP. The *subhorizontal white line* indicates the model tropopause altitude at the overpass time. Microwave Limb Sounder (MLS) retrievals of SO$_2$ (ppbv), HCl (ppbv) and ice-water content (IWC; mg/m^3) for several pressure levels (indicated top left in hPa) are plotted above the CALIOP data; these show clear enhancements in the volcanic cloud above 215 hPa.

p0090   The imaginary part of the refractive index, k, can be determined independently from the real part using either diffuse reflection (Patterson, 1981; Patterson et al., 1983; Winchester, 1998) or transmittance techniques (Pollack et al., 1973). In the reflection technique, k is determined by measuring the Kubelka–Munk coefficients of diluted ash samples. The samples are prepared by mixing known amounts of ash with highly reflective nonabsorbing powder (eg, barium sulfate, BaSO$_4$). The mixture is pressed into a pellet and placed inside an integrating sphere to measure the diffuse reflectance of the sample using a spectrometer as a filter (Winchester, 1998). The measured diffuse reflectance of the mixture is then inverted using the Kubelka–Munk theory to estimate the bulk absorption coefficient of the ash. Alternatively, k can be determined by measuring transmission spectra of a set of thin sections of varying thickness (30 μm–1 mm) and applying Beer's law to find the absorption coefficient independently of surface reflection or surface scattering effects (Pollack et al., 1973). The technique is sensitive to volume scattering effects, and opaque materials with high absorption coefficients cannot be measured. A new specular reflectance technique has been recently demonstrated for measuring k for aerosol particles resuspended on coarse (5-μm pores) and fine (0.4-μm pores) nucleopore filters in a broad spectral range from ~300 nm to 2.5 μm (Martins et al., 2009). The spectral absorption efficiency is derived from the measured normalized reflection spectra using an empirically modified Lambert–Beer law (Martins et al., 2009). The refractive index is derived using Mie or T-matrix theory and the measured size/shape distribution (Rocha-Lima et al., 2014).

VI. OBSERVING AIRBORNE ASH FROM SPACE

p0095   For volcanic ash, k varies by more than three orders of magnitude at UV wavelengths depending on ash composition and/or measurement technique (Fig. 4). To date, basaltic ash from Fuego volcano (Guatemala) ash has exhibited the strongest UV absorption, providing an upper boundary on k of $\sim$0.05 at 0.35 μm (Patterson et al., 1983), whilst obsidian materials with high silica content (>70%) typically show the lowest values of k (<0.001; Fig. 4). For comparison, k values for other aerosol types in the UV typically range from 0.01 to 0.03 for biomass burning aerosol (smoke), 0.007–0.013 for desert dust, and up to 0.004–0.012 for weakly absorbing aerosol (Torres

[**AU4**] et al., 2007). More recent k measurements exhibit less variability, with values typically between 0.0001 and 0.005

[**AU5**] at UV and blue wavelengths (Winchester, 1997; Rocha-Lima et al., 2014). Most recently, Rocha-Lima et al. (2014) measured the spectral optical properties of ash from the April–May 2010 eruption of Eyjafjallajökull (Iceland) in the UV to near infrared. They found peak values of k in the UV region and strong wavelength dependence, with k higher for smaller particles at UV wavelengths (perhaps indicating that UV measurements are more sensitive to fine ash). Although the UV k value found for Eyjafjallajökull ash is the same order of magnitude as previous labo-

[**AU6**] ratory measurements of Mt. Spurr volcanic ash (Krotkov et al., 1999), values were lower than measured for Mount St. Helens and Fuego ashes in the 1980s (Patterson, 1981; Patterson et al., 1983), consistent with its intermediate composition (trachyandesite; Sigmarsson et al., 2011). Rocha-Lima et al. (2014) also found no significant variation in k values derived from Mie theory (spherical particles) and the T-matrix method (spheroids), indicating no major impact of particle shape, as also observed by Krotkov et al. (1999b). Although the apparent variability in k (Fig. 4) suggests the possibility of discriminating ash composition by inverting satellite hyperspectral UV measurements, more measurements are needed to develop robust parameterizations of k as a function of ash composition for use in satellite retrievals.

p0100   The real part of the refractive index (n) can be determined by evaluating the Fresnel equation for nadir reflection of compressed pure ash samples (Pollack et al., 1973; Egan and Becker, 1969) or by using immersion techniques (eg, the Becke line technique) using liquids with known refractive indices (Wahlstrom, 1974; Ball et al., 2015). Values of n vary from 1.5 to 1.65 at UV wavelengths, typically decreasing with wavelength (Patterson, 1981). There are currently no methods for satellite retrievals of n.

s0040 **2.2.3 Volcanic Ash Particle Shape and Sizes**

p0105   Volcanic ash particles have a wide distribution of shapes and sizes, which complicates quantitative retrievals. The upper limit on ash particle sizes in a volcanic cloud is determined by sedimentation processes and depends on particle diameter and shape. For example, particles >50 μm in diameter fall out of an ash plume within few hours at rates of around $\sim$1 km/h, while particles of 1 μm in diameter fall out at a much slower rate of about 0.01 km/h (Bonadonna et al., 1998). However, fine ash can also be more rapidly removed from volcanic clouds, most likely by relatively poorly understood processes such as ash aggregation or ice nucleation (eg, Durant et al., 2009). Based on satellite studies, only about 1–2% of the total ash mass erupted falls into the 1–12 μm range that can remain airborne for a few days (Krotkov et al., 1999a; Rose et al., 2001). Since airborne ash particles are difficult to collect, often the only samples available for direct measurements (eg, of refractive index; Section 2.2.2) are taken from the ground, which may not accurately represent the characteristics of the ash fraction aloft detected from space. The grain size/shape distributions of volcanic ash can be analyzed using a variety of techniques, such as scanning electron microscope (SEM) analysis (eg, Rocha-Lima et al., 2014) or laser diffraction analysis (Riley et al., 2003).

s0045 **2.2.4 Hyperspectral Ultraviolet Volcanic Ash Retrievals**

p0110   The UV ash retrieval technique described in Section 2.2.1 was first developed using multispectral TOMS data, but could equally be applied to two channels of hyperspectral UV data (eg, from OMI, GOME-2, or OMPS). To date, there has been limited effort to exploit the full information content of hyperspectral UV measurements for volcanic ash retrievals, although the potential exists (Section 2.2.2) for discrimination of volcanic ash composition through inversion of hyperspectral data if more spectral refractive index measurements become available for a wide range of ash compositions.

p0115   The operational, multiwavelength OMI aerosol algorithm (OMAERO), which is distinct from the near-UV OMAERUV product, uses a spectral fitting approach that seeks to exploit the UV-to-visible OMI spectral coverage for aerosol characterization (Veihelmann et al., 2007). In this spectral range, there is sensitivity to aerosol absorption in the near-UV region, and to aerosol layer height in the near-UV and in the absorption band of the O_2–O_2 collision complex at 477 nm in the visible. These sensitivities allow OMAERO to identify realistic aerosol models that are used in the retrieval of aerosol extinction optical depth at several wavelengths in the range of 354–500 nm.

s0050

3. CASE STUDIES

p0120   The UVAI and similar products have been used to detect many volcanic ash clouds during the ∼37 years of satellite UV measurements by TOMS, GOME, SCIAMACHY, OMI, GOME-2, and OMPS. We highlight some recent, distinctive examples here (Figs. 2, 6, and 7); many others are documented on the NASA Global Sulfur Dioxide Monitoring website (NASA, 2015).

s0055 ### 3.1 The 2010 Eyjafjallajökull Eruption
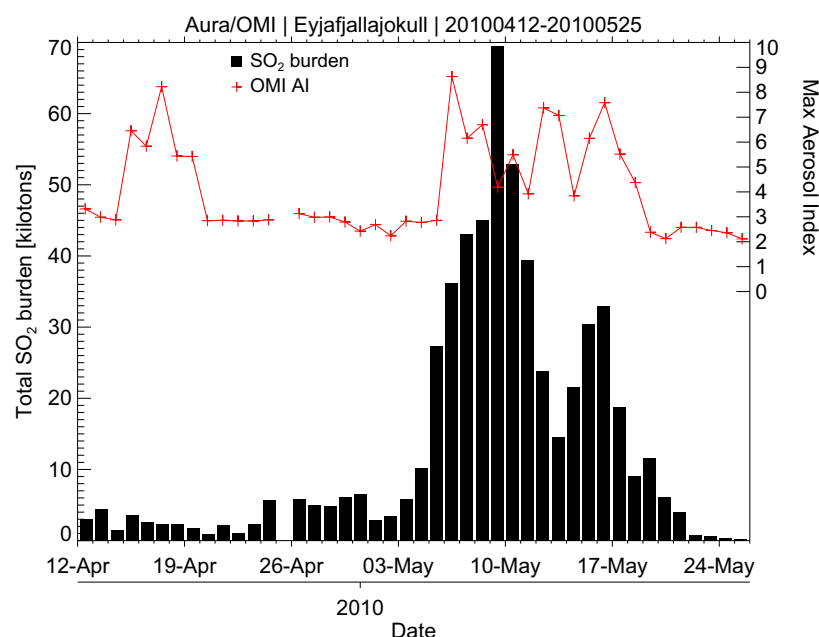
p0125   The April–May 2010 eruption of Eyjafjallajökull (Iceland) involved several weeks of continuous emissions of volcanic gases and ash to variable altitudes, leading to major impacts on aviation across Europe and worldwide, and generating renewed interest in the volcanic ash hazard to aviation (eg, Sammonds et al., 2010). The eruption has been studied in detail using several satellite datasets in the UV, visible, and IR (eg, Winker et al., 2012; Prata and Prata, 2012; Kahn and Limbacher, 2012; Pavolonis et al., 2013), but here we highlight the value of simultaneous OMI SO_2 and UVAI measurements for distinguishing eruptive phases (Fig. 6). The first explosive phase of the eruption in mid-April is characterized by high UVAI signals (indicating significant ash emissions) but relatively low SO_2 emissions (Fig. 6), reflecting the phreatomagmatic nature of the activity as magma erupted through the preexisting ice cap at the summit of Eyjafjallajökull. Glacial meltwater presumably scrubbed much of the SO_2 in the early emissions, whereas volcanic ash was generated by explosive interaction of magma and water. Following this explosive phase, in late April through early May, the UVAI signal diminishes, but SO_2 emissions increase (Fig. 6); this corresponds to a period of lava effusion at the surface when ash emissions were low (due to the absence of explosive activity) but SO_2 degassing continued. Then, on May 5–6, both ash and SO_2 emissions increase concurrently, indicating the onset of the second, magmatic explosive phase of the eruption driven by influx of new magma into the system (eg, Sigmarsson et al., 2011). Finally, the end of the eruption in late May is manifested by a reduction in UVAI as ash emissions ended, and residual degassing of SO_2 (Fig. 6).

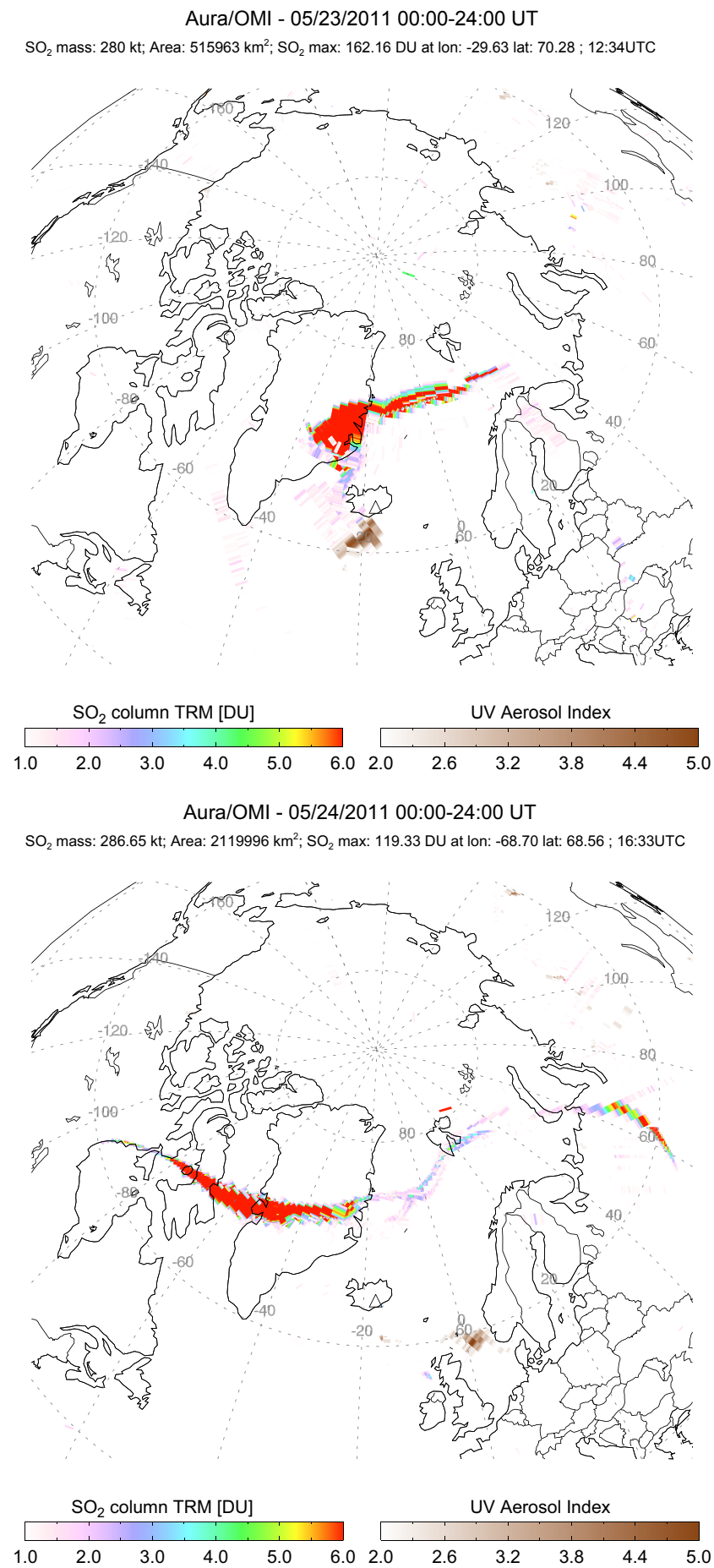s0060 ### 3.2 The 2011 Grimsvötn Eruption

p0130   Another Icelandic eruption, that of Grimsvötn on May 21, 2011, was larger than the Eyjafjallajökull eruption and injected SO_2 into the UTLS (Sigmarsson et al., 2013). However, coincident OMI SO_2 and UVAI measurements reveal a striking separation of ash-rich and SO_2-rich regions of the volcanic plume, with SO_2 at higher altitudes transported

f0035 FIGURE 6   Time-series of Ozone Monitoring Instrument (OMI) SO_2 and UVAI measurements between April 12 and May 25, 2010, during the 2010 eruption of Eyjafjallajökull (Iceland). Several eruption phases can be distinguished based on the relative abundance of SO_2 and volcanic ash.

Aura/OMI - 05/23/2011 00:00-24:00 UT

SO$_2$ mass: 280 kt; Area: 515963 km^2; SO$_2$ max: 162.16 DU at lon: -29.63 lat: 70.28 ; 12:34UTC

SO$_2$ column TRM [DU]   UV Aerosol Index

Aura/OMI - 05/24/2011 00:00-24:00 UT

SO$_2$ mass: 286.65 kt; Area: 2119996 km^2; SO$_2$ max: 119.33 DU at lon: -68.70 lat: 68.56 ; 16:33UTC

SO$_2$ column TRM [DU]   UV Aerosol Index

f0040 **FIGURE 7**   Coincident OMI observations of SO$_2$ and volcanic ash emitted by the May 2011 eruption of Grimsvötn (Iceland), showing striking separation of lower tropospheric ash and upper tropospheric/stratospheric SO$_2$ (Sigmarsson et al., 2013).

north of Iceland and lower tropospheric ash transported to the south and east, where it impacted surface-level air quality in southern Finland (Kerminen et al., 2011). Although separation of ash and SO_2 is commonly observed in volcanic eruption clouds (eg, Seftor et al., 1997; Schneider et al., 1999), this remains one of the best examples of the phenomenon recorded to date, with no detectable ash evident in the SO_2 cloud and vice versa. The cause of the highly efficient separation of SO_2 and ash remains uncertain, but given the wet nature of subglacial Grimsvötn eruptions, rapid ash sedimentation due to wet ash aggregation and ice nucleation seems plausible.

s0065   ## 3.3 The 2011 Cordón Caulle Eruption

p0135   The June 2011 eruption of Puyehue—Cordón Caulle (Chile) was notable for the longevity of the UVAI signal associated with the drifting ash cloud emitted during the initial explosive eruption (Fig. 2). The ash cloud was tracked using the OMI UVAI for over a week as it completed at least one global circuit of the southern hemisphere (the volcanic cloud eventually completed three circumpolar circuits), impacting aviation in South America, Australia, and New Zealand. In contrast, the UV SO_2 measurements were relatively poor due to the austral winter conditions (high solar zenith angle and high ozone column amounts), which clearly had less impact on the UVAI observations. UVAI anomalies related to volcanic ash clouds rarely persist for more than a few days; in this case, the longevity of the volcanic ash cloud may be attributable to small ash particle sizes generated by explosive fragmentation of highly silicic, rhyodacitic magma.

s0070   # 4. CONCLUSION

p0140   The UVAI is a powerful technique for daytime volcanic ash detection and tracking, particularly in the presence of clouds. The lack of nighttime data and geostationary UV measurements has limited the operational application of UV observations of volcanic ash. Coincident UV SO_2 and UVAI measurements have proved valuable for detecting magmatic eruptions and separation of ash and SO_2 in volcanic clouds. Quantitative UV ash retrievals have been demonstrated for some eruptions and compare favorably with IR ash retrievals, within the range of uncertainty of each technique. The major obstacle to wider application of UV ash retrievals is the paucity of measurements of ash optical properties for a range of volcanic ash compositions. More spectral refractive index measurements on fine volcanic ash are required for improved satellite-based retrievals of volcanic ash properties.

Non-Print Items

Abstract

Ultraviolet (UV) remote sensing of volcanic ash and other absorbing aerosols from space began with the launch of the first Total Ozone Mapping Spectrometer (TOMS) instrument in 1978. Subsequent UV satellite missions (TOMS, GOME, SCIAMACHY, OMI, GOME-2, OMPS) have extended UV ash measurements to the present, generating a unique multidecadal record. A UV Aerosol Index (UVAI) based on two near-UV wavelengths, equally applicable to multispectral (TOMS, DSCOVR) or hyperspectral (GOME, SCIAMACHY, OMI, GOME-2, OMPS) instruments, has been used to derive a unique absorbing aerosol climatology across multiple UV satellite missions. Advantages of UV ash measurements relative to infrared (IR) techniques include the ability to detect ash at any altitude (assuming no clouds), above clouds, and over bright surfaces, where visible and IR techniques may fail. Disadvantages include the daytime-only restriction and nonspecificity to silicate ash, since UV measurements are sensitive to any UV-absorbing aerosol, including smoke, desert dust, and pollution. However, simultaneous retrieval of sulfur dioxide (SO_2) abundance and UVAI provides robust discrimination of volcanic clouds. Although the UVAI is only semiquantitative, it has proved successful at detecting and tracking volcanic ash clouds from many volcanic eruptions since 1978. NASA A-Train measurements since 2006 (eg, CALIOP) have provided much improved constraints on volcanic ash altitude, and also permit identification of aerosol type through sensor synergy. Quantitative UV retrievals of ash optical depth, effective particle size, and ash column mass are possible and require assumptions of ash refractive index, particle size distribution, and ash layer altitude. The lack of extensive ash refractive index data in the UV−visible and the effects of ash particle shape on retrievals introduce significant uncertainty in the retrieved parameters, although limited validation against IR ash retrievals has been successful. In this contribution, we review UV ash detection and retrieval techniques and provide examples of volcanic eruptions detected in the ~37 year data record.